Journal of Power Sources 195 (2010) 39–45

Contents lists available at ScienceDirect

Journal of Power Sources

journal homepage: www.elsevier.com/locate/jpowsour

Direct dimethyl-ether proton exchange membrane fuel cells and the use of heteropolyacids in the anode catalyst layer for enhanced dimethyl ether oxidation

Jack R. Ferrell III, Mei-Chen Kuo, Andrew M. Herring*

Department of Chemical Engineering, Colorado School of Mines, Golden, CO 80401, USA

ARTICLE INFO

Article history:
Received 14 May 2009
Received in revised form 4 July 2009
Accepted 6 July 2009
Available online 14 July 2009

Keywords:
PEM fuel cell
Heteropoly acid
Dimethyl ether
Electrocatalysis

ABSTRACT

In this study, polarization and impedance experiments were performed on a direct dimethyl ether fuel cell (DMEFC). The experimental setup allowed for independent control of water and DME flow rates. The DME flow rate, backpressure, and water flow rate were optimized. Three heteropolyacids, phosphomolybdic acid, $H_3PMo_{12}O_{40}$. (HPMo), phosphotungstic acid, $H_3PW_{12}O_{40}$, (HPW), and silicotungstic acid, $H_4SiW_{12}O_{40}$, (HSiW) were incorporated into the anode catalyst layer in combination with Pt/C. Both HPW-Pt and HSiW-Pt showed higher overall performance than the Pt control. Anodic polarizations were also performed, at 30 psig, Tafel slopes of 67 mV dec^{-1}, 72 mV dec^{-1}, and 79 mV dec^{-1} were found for HPW-Pt, HSiW-Pt and the Pt control, respectively. At 0 psig, the Tafel slopes were 56 mV dec^{-1}, 58 mV dec^{-1}, and 65 mV dec^{-1} for HPW-Pt, HSiW-Pt and the Pt control. The trends in the Tafel slope values are in agreement with the polarization data and the electrochemical impedance spectroscopy results. The addition of phosphotungstic acid more than doubled the power density of the fuel cell, compared to the Pt control. When the maximum power density obtained using the HPW-Pt MEA is normalized by the mass of Pt used, the optimal result, 78 mW mg^{-1} Pt, the highest observed at 30 psig and 100 °C to date.

1. Introduction

Proton exchange membrane (PEM) fuel cells are very attractive energy conversion devices, but the fuel of choice, gaseous hydrogen, which has a very high specific energy density, also has a very poor volumetric energy density, 33,500 kWh tonne^{-1} and 600 kWh m^{-3} at 200 bar respectively [1]. It is, therefore of interest to investigate the use of easily condensable fuels for PEM fuel cells. Electro-oxidation of non-hydrogen fuels in PEM fuel cells typically suffers from undesirably high overpotentials compared to hydrogen. Much work has gone into the research and development of the direct methanol fuel cell (DMFC), but in comparison much less attention has been paid to other potential C_1 fuels. Commercialization of the DMFC has been hindered by efficiency losses due to fuel crossover, the slow kinetics of methanol electro-oxidation, and water management. Methanol is also toxic and highly miscible with water; this has slowed real-world applications of the DMFC. Dimethyl ether (DME) is the simplest ether, with the chemical formula CH_3OCH_3. DME is currently used as an aerosol and propellant for spray paints and is a potential replacement for diesel fuel [2,3]. DME is a desirable candidate for diesel replacement because it contains no C–C bond, and thus particulate formation can be dramatically reduced and it has been proposed to be a useful intermediate from a petroleum based economy to a hydrogen economy [3]. For fuel cell use, the number of electrons transferred for complete oxidation is 12; this results in a reduced theoretical fuel requirement of DME, when compared to methanol with 6 electrons transferred, and hydrogen with 2 electrons

DME has a vapor pressure between butane and propane, making storage as a liquid simple with existing technology. In this manner, DME combines the ease of delivery of hydrogen (i.e. no pumps required) with the high energy density of a liquid fuel such as methanol [3]. DME also has a low toxicity; it is not toxic upon skin contact as is methanol. DME is less polar than methanol, with dipole moments of 1.30 D for DME and 1.7 D for methanol [4]. For this reason, DME is much less soluble in water than methanol, with DME having a solubility of 76 g L^{-1} of water. Since DME is only slightly soluble in water, the crossover is expected to be much less than that of methanol [2]. Reduced crossover is seen in the literature via a consistently higher open circuit potential for the DMEFC compared to the DMFC. For these reasons, DME is a promising fuel for use in PEM fuel cell systems and since the original report in 1998 [5], a number of reports are appearing in the recent literature [2,6–14].

On the anode of a DMEFC, the following oxidation reaction takes place:

$$CH_3OCH_3 + 3H_2O \rightarrow 2CO_2 + 12H^+ + 12e^- \quad (1)$$

* Corresponding author. Tel.: +1 303 384 2082; fax: +1 303 273 3730.
E-mail address: aherring@mines.edu (A.M. Herring).

0378-7753/$ – see front matter © 2009 Elsevier B.V. All rights reserved.
doi:10.1016/j.jpowsour.2009.07.011

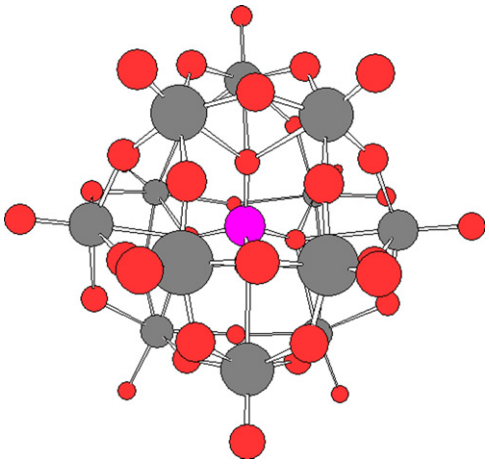

Fig. 1. Structure of the Keggin Ion, $[XM_{12}O_{40}]^{x-8}$.

For DME electro-oxidation to occur, the molar flow rate of water must be at least three times that of DME. This 3:1 molar ratio can be hard to achieve, depending on how the system is set up. If DME is to be fed to the fuel cell as a liquid, the solubility limits the solution to a maximum concentration of 1.65 M at STP [2]. If DME is to be fed as a gas, the most common way of humidifying the fuel has been to bubble it through water. This also has limits. For example, if bubbling DME at 100 °C, the pressure must be at least 20 psi to satisfy the 3:1 molar ratio [2]. On the cathode, the oxygen reduction reaction occurs:

$$12H^+ + 12e^- + 3O_2 \rightarrow 6H_2O \quad (2)$$

Combining the two half-cell reactions, the theoretical open circuit voltage of the DMEFC is 1.18 V, very similar to methanol and hydrogen [14]. In the DMEFC literature, is has been shown that the adsorption of DME on a Pt surface is non-trivial and dependent on potential [14]. Electrochemical investigations in aqueous solution reveal that DME electro-oxidation on Pt occurs preferentially at low pH, and not at all under basic conditions, with protonation of the oxygen atom playing a key role and a reaction scheme that ultimately goes through adsorbed CO [15–18]. Under conditions of higher temperature, >90 °C and pressure Pt–Ru shows enhanced electrochemical oxidation of DME [12]. However, not only is Ru an extremely rare metal but, Pt–Ru has material stability issues and it has been shown that Ru can cross through the membrane and deposit on the cathode electrode [19].

We have previously shown that the heteropoly acids (HPAs) can enhance the performance of the catalyst layer for PEM fuel cells [20–23] and that significant improvements can be seen for the oxidation of both CO and methanol. It has recently been reported that DME electro-oxidation can be enhanced on Pt by the HPA, 12-phosphomolybdic acid [24]. HPAs are desirable in the catalyst layer not only because they have been shown to have catalytic activity for the necessary reactions, but also because they have a high protonic conductivity [25]. Interestingly in this context the HPA have a very strong affinity for ethers and the isolation of HPA etherates is often used in the synthesis of the free acids of HPAs [26].

The HPAs are a subset of the polyoxometalates in which the polyoxometalate units surround a central heteroatom. These materials have attracted considerable attention for catalytic applications [27]. HPAs are very strong Bronsted acids, and they also exhibit fast reversible multielectron redox behavior under mild conditions. The acid–base and redox behavior can be widely varied by changing the chemical composition of the HPA. These properties make HPAs attractive candidates for redox catalysts in electrochemical processes. The Keggin HPA, shown in Fig. 1 can be represented by the formula $[XM_{12}O_{40}]^{x-8}$ [28]. The structure of this molecule was resolved using XRD by Keggin [29]. At the center of the compound is the heteroatom X (typically Si, P, etc.), which has four oxygen atoms attached forming a tetrahedron. The oxidation state of the heteroatom is represented by *x* in the formula above. *M* is the addenda atom, which is usually Mo or W. The central hetroatom in a tetrahedral environment is surrounded by 12 octahedra of composition MO_6. The oxygen atoms are shared, except for 12 terminal oxygen atoms attached to only one addenda atom [26].

Here we demonstrate that, after careful optimization of a DMEFC, that a HPA doped Pt containing catalyst layer can enhance the utilization of DME in a DMEFC.

2. Experimental

2.1. Materials

Phosphomolybdic acid, $H_3PMo_{12}O_{40}$ (HPMo), phosphotungstic acid, $H_3PW_{12}O_{40}$ (HPW), and silicotungstic acid, $H_4SiW_{12}O_{40}$, (HSiW) were used as received (Sigma–Aldrich). The membrane electrode assemblies (MEAs) in this study were constructed from Nafion® 112 or 117 (Ion Power). The ionomers were cleaned and protonated by first boiling in 3% H_2O_2 for 1 h, followed by 1 h of boiling in DI water, 1 h of boiling in 0.5 N H_2SO_4, and finally 1 h of boiling in DI water [30]. Following this treatment the membranes were stored in DI water in the dark before use. A 5 wt% Nafion® solution (Sigma–Aldrich) was used in the catalyst layer. Electrode Los Alamos Type (ELAT) gas diffusion layers (BASF Fuel Cell, Inc.) containing 0.5 mg Pt cm^{-2} (20% Pt on Vulcan XC-72 carbon) were used as cathode gas diffusion electrodes. These ELAT electrodes were also used on the anode for optimization experiments. The catalyst used on the anode in the heteropoly acid study was a 20% Pt on Vulcan XC-72 powder (BASF Fuel Cell, Inc.). This anode catalyst was applied to the microporous layer of a 10 BB paper electrode (SGL carbon).

2.2. MEA fabrication

Catalyst inks were airbrushed onto paper electrodes to make gas diffusion electrodes. Catalyst inks were made in a syringe by combining the desired catalyst, methanol, and Nafion® solution. For inks including HPAs, the HPA was simply added to the ink. Nafion® solution was added such that the Nafion® solids were 25% of the total mass of Pt/C and Nafion® solids in the ink. Methanol was added in an amount that was ten times the mass of Pt/C in the ink. The ink was mixed in the syringe using a Crescent Wig-L-Bug amalgamator for 2 min and then placed in an ultrasonic bath for 20 min.

A syringe pump was used to deliver the ink to an *X*–*Y* plotter that worked as an airbrush. The *X*–*Y* plotter applied coats of ink to the paper electrode in a serpentine pattern. The number of coats was set such that a Pt loading of 0.30 ± 0.02 mg cm^{-2} and an HPA loading of 1.00 ± 0.05 mg cm^{-2} was obtained, and the actual samples were weighed to ensure the correct loading was used. Two electrodes were made from each ink and both were tested to ensure reproducibility. Following airbrushing, the electrodes were placed under a 250 W heat lamp to evaporate the methanol solvent in the catalyst layer. Only the anode electrodes were fabricated in this manner, and only anode electrodes contained HPAs. Pt ELAT electodes loaded at 0.5 mg Pt cm^{-2} were used on the cathode. Once the anode and cathode electrodes were fabricated, they were cut into squares with an area of 5.5 cm^2 each. These electrodes were hot pressed to either side of a cleaned Nafion® 117 membrane, using a digital combo multi-purpose press, DC14 (GEO Knight & Co. Inc.). Pressing conditions used were 135 °C at 80 psig for 90 s.

2.3. Electrochemical measurements

The DMEFC test stand consists of a pump, vaporizer, fuel cell hardware, backpressure regulators, water traps, a humidifier and mass flow controllers. A pump is used to pump water from a reservoir to the vaporizer. The pump is an isocratic HPLC pump (Chrom Tech—model ISO-100 digital). The vaporizer consists of quarter-inch Swagelok tubing that is wrapped with heat rope. Fine stainless steel mesh was packed inside the tubing to provide contact area for the phase change to occur on. This vaporizer has been calibrated for the respective water flow rates. DME is fed via a mass flow controller. The DME and water streams join at a junction, and then go directly to the anode. The fuel cell hardware (Fuel Cell Technologies, Inc.) is a single cell with area 5 cm^2 and single-serpentine flow fields. The fuel cell was run at 100 °C. The effluent from the fuel cell first travels through two backpressure regulators, which were purchased from Swagelok. The system has been run with 30 psig backpressure and at ambient pressure. After the backpressure regulators, the effluent goes through water traps, which separate out any liquid that has condensed in the exit lines. The remaining gas is then vented. Oxygen is fed to the cathode using a modular gas handling system (Lynntech industry Inc. GMET/H). The flow rate is 0.2 l min^{-1}, and the flow was controlled using FC Power software (Lynntech Industry Inc.). The oxygen then travels through a gas humidity bottle (Fuel Cell Technologies Inc.) and then to the fuel cell. The humidity bottle was kept at 80 °C.

To perform polarization experiments on the DMFC, an MSTAT4+ multi-potentiostat (Arbin Instruments) was used to manipulate cell voltage or current. Prior to the polarization experiments, the MEA was conditioned for 24 h at 30 psig. The conditioning process consisted of alternating potentiostatic holds at 0.35 V and 0.15 V for 30 min each. For polarization measurements, the cell is allowed to remain at open circuit for 5 min, then the potential is stepped down in 50 mV increments, with the cell remaining at each potential for 2 min. In the measurement of anodic polarization curves, nitrogen is fed to the cathode which acts as a pseudo-reference electrode. In this experiment, the potential was scanned from open circuit to more positive potentials, in 50 mV increments, until a limiting current was reached. Electrochemical impedance spectroscopy (EIS) experiments were performed using a Scribner 850C Compact Fuel Cell Test System and the associated Fuel Cell software. The Scribner 850C contains both an electronic load and a frequency response analyzer. Galvanostatic EIS was performed from 10,000 Hz to 0.1 Hz, taking data points at 15 steps dec^{-1}. The amplitude of the AC current was taken as 5% of the DC current. The impedance extrapolated to zero perturbation frequency gives a value for the resistance of the MEA; this value was found to match the resistance taken from the slope of the steady state polarization curve, providing evidence that the measured impedance was free from instrumental artifacts. The experimental data was fit using nonlinear least-squares fitting software (ZView, Scribner Associates, Inc., USA).

3. Results and discussion

3.1. Development of experimental conditions

DMEFC fuel cells are still a relatively new technology and so it is first necessary to vary the operating conditions. In this section, all MEAs used consisted of standard Pt ELATs (0.5 mg Pt cm^{-2}) on anode and cathode. Our experimental setup is similar to that of Haraguchi et al. [12]. As stated above, other previous studies have either used a liquid stream with DME dissolved in water [4,6–9,13,14] or used gaseous DME that has been saturated with water [2,4,6,10,11,13]. Both of these methods have their limitations. In the setup used here, a gaseous water stream is simply mixed with the gaseous DME stream. This allows independent control of both DME and water flow rates.

Many different conditions of backpressure, water flow rate, and DME flow rate were tested. The best combination of conditions was used for the HPA study, which is presented later in the paper. Unless otherwise noted, the cell temperature was maintained at 100 °C. 0.2 l min^{-1} of oxygen was supplied to the cathode. The cathode humidifier was run between 80 and 100 °C, at both ambient pressure and 30 psig, and no difference in performance was seen between these two temperatures. This shows that the performance was limited by processes occurring on the anode, as the operating conditions at the cathode had no effect on cell performance. We first investigated the effect of backpressure, data not shown. The addition of 30 psig of backpressure increased the performance of the DMEFC. This effect of pressure has been documented in two previous studies in the literature [4,12]. As stated in previous studies, enhanced pressure on the anode is thought to enhance DME adsorption on the electrocatalyst surface.

The DME flow rate was also varied, in combination with the water flow rate. DME flow was either 100 or 200 sccm. The water flow rate was varied between 0.6 ml min^{-1} and 1.8 ml min^{-1}. It was found that higher DME flow rates do not necessarily lead to better performance. It is the water to DME ratio that is important. The effect of water for the DMEFC at 30 psig, with 100 sccm of DME fed to the anode, is shown in Fig. 2. Interestingly at higher pressures, e.g. 65 psig little difference has been observed on Pt [12]. A water flow rate of 0.6 ml min^{-1} corresponds to a water:DME molar ratio of 7.5. A ratio of 3 or higher is stoichiometrically required. At a water flow rate of 1.2 ml min^{-1}, the water:DME ratio is 14.9. In this case, a doubling of current is seen by simply feeding more water to the cell. While both of these water flow rates exceed the stoichiometric requirement, more than doubling the required amount of water shows the best results.

At the lowest pressures, feeding more water actually hinders performance. At 0 psig and 100 sccm of DME, the water flow rate was varied between 0.6 ml min^{-1}, 1.2 ml min^{-1}, and 1.8 ml min^{-1}, as seen in Fig. 3. Upon changing the water flow from 0.6 to 1.2 ml min^{-1}, a dramatic improvement is seen. This is moving from a water:DME ratio of 7.5–14.9. Increasing the water flow further to 1.8 ml min^{-1}, with a water:DME ratio of 22.4, results in lower currents than when using 1.2 ml min^{-1}. Based on this, there does appear to be an ideal amount of water to feed to the cell to maximize DME electro-oxidation. Based on this study, the water:DME ratio needs to be significantly higher than that which is required stoichiometrically. We suggest that excess water, above the stoichiometric requirement, is beneficial because a surplus of water on the catalyst surface will lead to enhanced DME utilization. Since

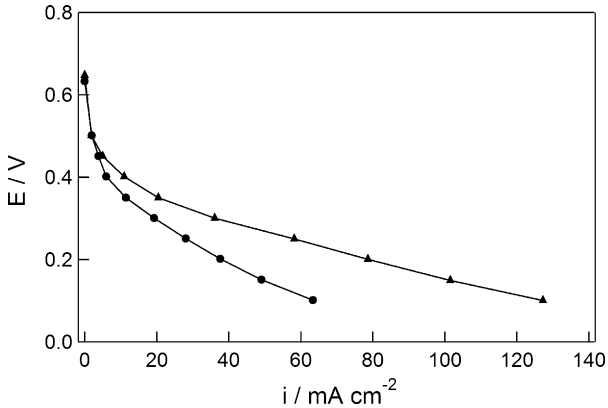

Fig. 2. Effect of water flow rate. Cell at 30 psig, 100 °C. 100 sccm of DME. Water flow rate: 0.6 ml min^{-1} (-●-); 1.2 ml min^{-1} (-▲-).

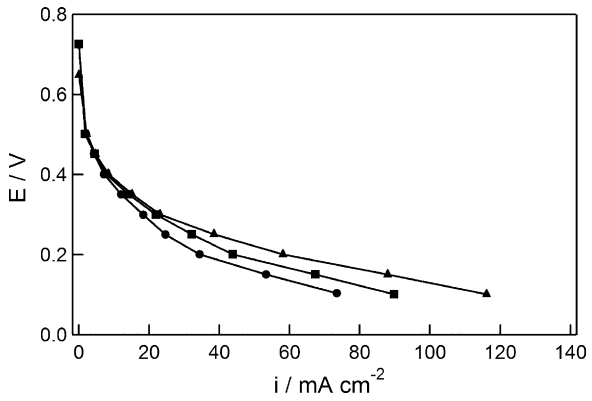

Fig. 3. Effect of water flow rate. Cell at 0 psig, 100 °C. 100 sccm of DME; water flow rate: 0.6 ml min^{-1} (-●-); 1.2 ml min^{-1} (-▲-); 1.8 ml min^{-1} (-■-).

DME is flowing, the residence time is finite, and excess water on the catalyst surface will allow for more facile oxidation of DME when it adsorbs on the surface. As stated above, 200 sccm was also used as a flow rate for DME. It is worth noting that all results when using 200 sccm were lower than when using 100 sccm. This is true even when the two DME flow rates had comparable water: DME ratios. Clearly the system needs to be optimized not only for the –OH coverage on the catalyst, but, also for the mass transport of water and DME through GDEs optimized with hydrophobic and hydrophilic components for more conventional fuel cells. Presumably future DME fuel cells will include engineering approaches that optimize the GDE for the fuel rather than the DME/water ratios for the GSE.

It is expected that crossover should be less of an issue in the DMEFC compared to the DMFC as DME is much less polar than methanol. In the literature, there is conflicting information regarding DME crossover. Muller et al. [14] found that the amount of DME crossover is significant, typically being equivalent to about 100 mA cm^{-2}. The DME concentration in the cathode outlet was monitored, and found to be the same when feeding either O_2 or H_2 to the cathode. Also, only trace amounts of CO_2 were found in the cathode outlet. From this, the authors concluded that DME is not oxidized at the cathode [14]. In another study, Mench et al. [2] found lower fuel cell performance when using Nafion® 115 than when using Nafion® 117. The open circuit voltage also dropped over 100 mV when going to the thinner 115 membrane and no appreciable performance was seen when using a Nafion® 112 membrane [2]. These results show that DME is in fact oxidized at the cathode.

In this study, both Nafion® 112 and 117 were both used. This effect of membrane thickness can be seen in Fig. 4. First, the open circuit potential for Nafion® 112, 0.51 V, is 140 mV lower than that of Nafion® 117, which is 0.65 V. In this manner, these results agree with

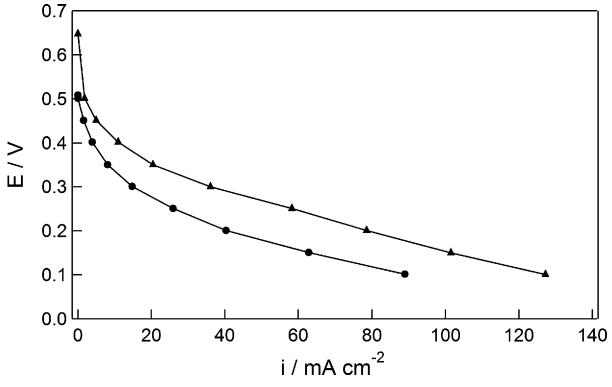

Fig. 4. Effect of membrane thickness. Cell at 30 psig, 100 °C. 100 sccm of DME. Water flow rate: 1.2 ml min^{-1}. Nafion® 112 (-●-); Nafion® 117 (-▲-).

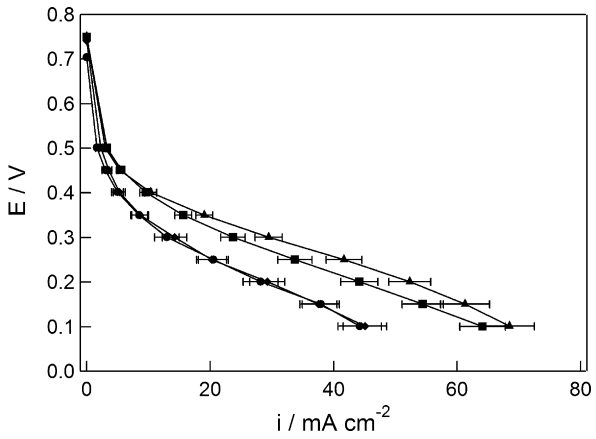

Fig. 5. DMEFC cell polarization. Cell temperature: 100 °C, 0 psig backpressure; DME flow rate: 100 sccm; water flow rate: 1.2 ml min^{-1}. Pt control (-●-); HPMo-Pt (-♦-); HSiW-Pt (-■-); and HPW-Pt (-▲-).

those of Mench et al. [2], indicating that DME does crossover and is oxidized at the cathode. However, even though Nafion® 117 showed the best performance, we did see sufficient current when using a Nafion® 112 membrane. From these experiments, the experimental conditions were chosen as follows: cell temperature 100 °C, DME flow rate 100 sccm, water flow rate 1.2 ml min^{-1}, cathode O_2 flow rate was 200 sccm humidified at 80 °C, and Nafion® 117 was used as the membrane. Backpressures of both 0 psig and 30 psig were compared.

3.2. Polarization results using heteropolyacids

Three commercially available HPAs, HPMo, HPW, and HSiW, were combined with Pt and applied to the anode catalyst layer. These HPA were chosen, not just because they are commercially available, but also as the HPA with the lightest heteroatom elements that are naturally inclined to the tetrahedral environment, of the Keggin structure, such as P or Si, are the most stable. HSiW is known to be more acidic and the molybdenum analogue is known to have more facile redox chemistry allowing us to probe more chemistry in the DME fuel cell. At 0 psig, the polarization results can be seen in Fig. 5. Phosphotungstic acid (HPW) and silicotungstic acid (HSiW) both lead to improvements when added to the anode catalyst layer. Interestingly the MEA incorporating phosphomolybdic acid (HPMo) only had similar currents as the Pt control, compared to *ex situ* solution testing that indicated that an improvement should have been observed [24]. Also, HPW appears to have slightly better results than HSiW. The use of HPW as an electrocatalyst for DME oxidation is an original result, there is no precedent for using HPW for DME electro-oxidation. However, there is precedent for HPW acting as an electrocatalyst for other small molecules, such as methanol [22,31] and CO [32]. At 0.1 V, the current densities are 44 mA cm^{-2} for the Pt control, 45 mA cm^{-2} for HPMo-Pt, 64 mA cm^{-2} for HSiW-Pt, and 68 mA cm^{-2} HPW-Pt. From the shape of the polarization curve, it is seen that the activation overpotential dominates, as the curve drops very steeply at low currents. The polarization curves at 30 psig are shown in Fig. 6. Again, it is seen that both HPW and HSiW lead to overall improvements beyond experimental error. At 0.1 V, the current densities are 82, 98, 125, and 187 mA cm^{-2} for the Pt control, HPMo-Pt, HSiW-Pt, and HPW-Pt, respectively. Thus, at these conditions, the addition of phosphotungstic acid has more than doubled the performance of the DMEFC. Inclusion of HPMo into the anode catalyst layer leads to only slightly higher currents than the Pt control. For this reason, HPMo was not included in further experimentation. For time periods of up to 2 days, no HPA leaching occurred, and no drop in performance was seen.

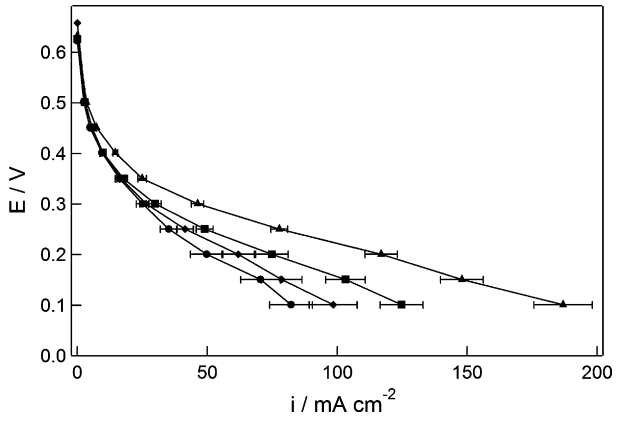

Fig. 6. DMEFC cell polarization. Cell temperature: 100 °C, 30 psig backpressure; DME flow rate: 100 sccm; water flow rate: 1.2 ml min^{-1}. Pt control (-●-); HPMo-Pt (-♦-); HSiW-Pt (-■-); HPW-Pt (-▲-).

To separate the improvements in anode electrocatalysis from mass transport and oxygen reduction effects, anodic polarizations were performed to analyze the anodic half-cell. In doing these tests, $N_{2(g)}$ was fed to the cathode, and a potentiostat was used to polarize the anode and force DME electro-oxidation. At ambient pressure, the anode polarization curves are shown in Fig. 7. The same trends are seen as for the DMEFC cell polarization; HPW-Pt shows the highest currents, while HSiW-Pt still produces currents greater than the control. In the inset on Fig. 7, the same data is shown in semi-log format. Tafel slopes were extracted from this data between 0.3 V and 0.5 V. At 0 psig, the Tafel slopes were 65 mV dec^{-1} for the Pt control, 58 mV dec^{-1} for HSiW-Pt, and 56 mV dec^{-1} for HPW-Pt.

Anodic polarization experiments were also performed at 30 psig, and can be seen in Fig. 8. Again, similar behavior is seen as in the cell polarizations. For this data at 30 psig of backpressure, Tafel slopes were taken in the range between 0.4 V and 0.6 V. Values of the Tafel slopes are 79 mV dec^{-1} for Pt control, 72 mV dec^{-1} for HSiW-Pt, and 67 mV dec^{-1} for HPW-Pt. Also, from Figs. 7 and 8, it is apparent that 300–400 mV of overpotential is required to oxidize DME under these conditions. After this overpotential requirement is met, DME is oxidized at a fairly fast rate, since the Tafel slope values are relatively low. In fact, the theoretical Tafel slope value is 64 mV dec^{-1} for a 2 electron transfer, assuming an α value of 0.5. Liu et al. [17] found a Tafel slope value of 65 mV dec^{-1} for DME electro-oxidation when using a Pt/C catalyst in 1 M sulfuric acid. In this context, the Tafel slope values measured here are consistent with the *ex situ* experiments.

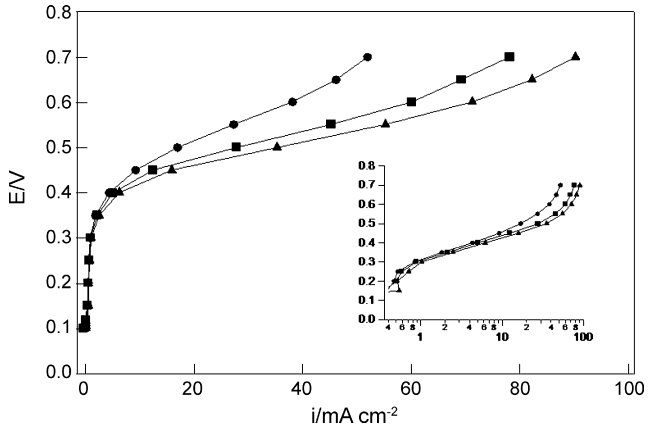

Fig. 7. Anodic polarization. Cell temperature: 100 °C; DME flow rate: 100 sccm, 0 psig of backpressure. Pt control (-●-); HSiW-Pt (-■-); HPW-Pt (-▲-). Inset: Tafel plot.

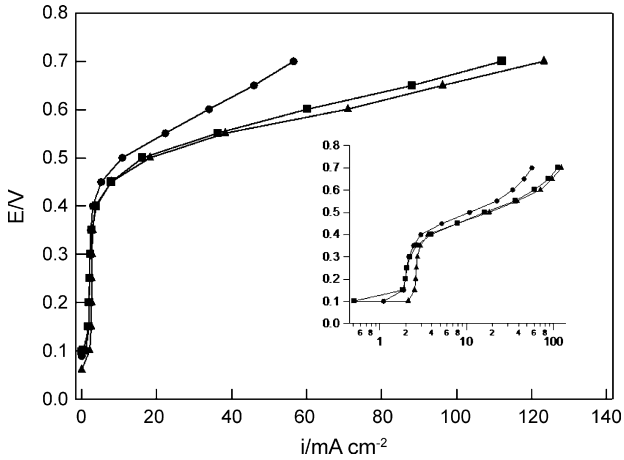

Fig. 8. Anodic polarization. Cell temperature: 100 °C; DME flow rate: 100 sccm, 30 psig of backpressure. Pt control (-●-); HSiW-Pt (-■-); HPW-Pt (-▲-). Inset: Tafel plot.

To compare this work to other DMEFC studies, we have normalized the maximum power density seen by the amount of Pt used, yielding a metric with units of mW mg^{-1} Pt. We have compared our results to available performance data in the literature where a PEM based DMEFC reported a polarization curve. Values generally range from 6 to 30 mW mg^{-1} Pt depending upon the conditions employed which unfortunately vary dramatically [2,4,6–11,13,14]. The best performance reported in the literature was that of Haraguchi et al., with a DMEFC running at 130 °C and 65 psig, 130 mW mg^{-1} Pt was obtained for a Pt catalyst [12]. There is also one study of a DMEFC at higher temperatures using an anhydrous proton conductor. At 300 °C, the fuel cell produced 10 mW mg^{-1} Pt [33]. In our study, the best results seen were for HPW-Pt at 30 psig, 100 °C where 78 mW mg^{-1} Pt was obtained which is higher than that observed by Haraguchi et al., 70 mW mg^{-1} Pt, for pure Pt at the same temperature, but at the higher pressure of 65 psig. The high power density per mg of Pt used is attributed to the experimental setup, and also to the use of HPAs. As observed with the use of HPA in DMFC fuel cells a 10% improvement can be obtained when an optimized HPA is incorporated into the catalyst layer [22].

3.3. Impedance results using heteropolyacids

From the polarization results, it is clear that the inclusion of various heteropolyacids improves the performance of the DMEFC. To make these results more meaningful, electrochemical impedance spectroscopy (EIS) was performed in an attempt to find out how the heteropolyacid increases the current coming out of the DMEFC. Galvanostatic EIS was performed at both 0 psig and 30 psig at four different points along the polarization curves: 9.1, 18.2, 27.4, and 36.5 mA cm^{-2}. These points were chosen such that an impedance spectrum was taken in each characteristic portion of the polarization curve. At least one impedance spectrum was recorded in the activation region, one in the ionic region, and one in the transport region. An equivalent circuit model, shown in Fig. 9, was used to fit the data. Other equivalent circuit models were tested, including one that used ideal capacitors in place of the constant phase

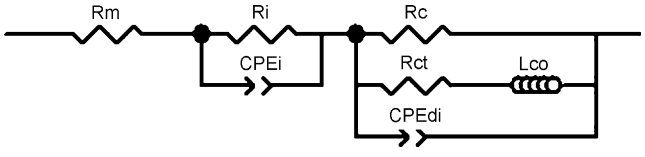

Fig. 9. Equivalent circuit used for modeling the electrochemical impedance data.

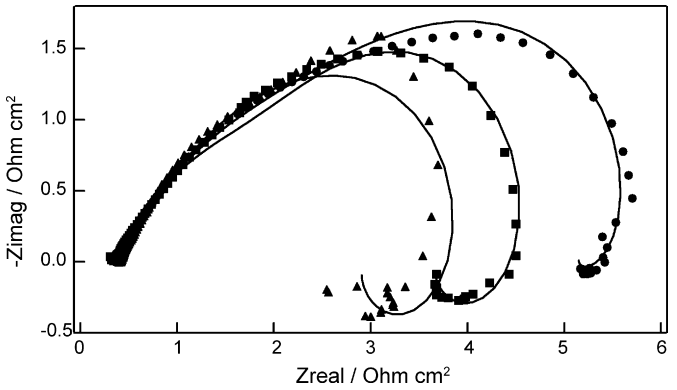

Fig. 10. Impedance at 30 psig and 36.5 mA cm^{-2}. Pt control (-●-); HSiW-Pt (-■-); HPW-Pt (-▲-).

Table 1
Equivalent circuit modeling parameters for the DMEFC at 30 psig.

mA cm^{-2}	R_m (Ohm cm^2)	R_i (Ohm cm^2)	$CPE_{i\text{-}Q}$ (F/cm^2)	$CPE_{i\text{-}p}$ (F/cm^2)
Pt control				
9.1 mA cm^{-2}	0.36	0.49	0.026	1
18.2 mA cm^{-2}	0.35	0.49	0.015	1
27.4 mA cm^{-2}	0.37	0.47	0.022	0.60
36.5 mA cm^{-2}	0.34	0.46	0.016	0.62
HSiW-Pt				
9.1 mA cm^{-2}	0.34	0.36	0.018	1
18.2 mA cm^{-2}	0.33	0.36	0.023	1
27.4 mA cm^{-2}	0.33	0.32	0.027	0.61
36.5 mA cm^{-2}	0.35	0.30	0.018	0.65
HPW-Pt				
9.1 mA cm^{-2}	0.32	0.21	0.021	1
18.2 mA cm^{-2}	0.32	0.20	0.027	0.71
27.4 mA cm^{-2}	0.34	0.17	0.023	1
36.5 mA cm^{-2}	0.34	0.15	0.015	1

elements in Fig. 9. Also, an equivalent circuit model that did not include parameters to represent the interfacial region was tested. However, the model shown in Fig. 9 provided the best fit of all the models tested. In the equivalent circuit model, R_m represents the membrane resistance; R_i represents the resistance of the interface between the membrane and catalyst layer; CPE_i models capacitive properties of this interface. R_c is the resistance of the solid phase of the catalyst layer, in combination with the non-inductively coupled resistance to charge transfer. R_{ct} is the resistance to charge transfer that is coupled to an inductance [22]. L_{co} is the inductance. Finally, a constant phase element, CPE_{dl}, models the capacitive characteristics of the porous electrode. A more complete description of this model is available [22].

A representative Nyquist plot, at 30 psig of backpressure, can be seen below in Fig. 10. The impedance results and the polarization results both show that the presence of HPAs leads to enhanced current densities. This is seen in the impedance results via a decreased semicircle width in the Nyquist plots. Thus, the impedance and polarization results both show that HSiW and HPW lead to statistically significant improvements over the Pt control, with phosphotungstic acid having the greatest effect. Impedance spectra at other current densities showed the same trends, consistently matching the polarization results.

As seen in Fig. 10, the equivalent circuit model fit is optimal, and deviates further from experimental data upon moving to lower frequencies. This effect has been documented in the literature [34]; the spectrum is smooth for low frequencies, and the spectrum has significant scatter at higher frequencies. Roy and Orazem found the scattering to be due to flooding of the single cell, due to the fact that the characteristic frequency associated with water droplet formation and growth matches the lower frequencies used in EIS [34]. Flooding of the cell is only one possibility for the noisy data at low frequencies. The data could also be noisy simply because the system is relatively unstable, due to the high overpotential required for DME electro-oxidation, and because the current densities reached with the DMEFC are low.

As seen in Fig. 10, the fit is very good at high frequencies; however, the data cannot be trusted upon moving to lower frequencies. This was also very evident upon inspection of the values of the equivalent circuit parameters. These values only made physical sense for the areas of the model representing the membrane resistance, and the interfacial region. At low frequencies, the values were scattered, and often physically unreasonable. For this reason, only the equivalent circuit parameters associated with high frequencies are reported, Table 1. To start, all values of membrane resistance, R_m, are very similar, having values between 0.32 and 0.37 Ω cm^2, as would be expected as we have, in theory, not perturbed the membrane here. This shows that the incorporated HPAs are not leaching into the membrane and increasing membrane conductivity. Thus, the higher current densities seen when using HPAs are due to processes occurring only in the catalyst layer and the interface between the catalyst layer and the membrane. Compared to the Pt control, the interfacial resistance, R_i, is consistently lower when HPAs are present. The values of R_i range between 0.46 and 0.49 Ω cm^2 for the control, 0.30 to 0.36 Ω cm^2 for HSiW-Pt, and 0.15–0.21 Ω cm^2 for HPW-Pt. These trends scale with the polarization results, with HPW-Pt showing the greatest effect. $CPE_{i\text{-}Q}$ is the admittance of the constant phase element which represents the capacitive nature of the interfacial region. Values of $CPE_{i\text{-}Q}$ 0.015 and 0.027 for all MEAs tested. No clear trend is seen in $CPE_{i\text{-}Q}$ values; however, this constant phase element was necessary to obtain a satisfactory fit, if even in the high frequency region. Finally, $CPE_{i\text{-}p}$ is the adjustment parameter for this constant phase element. $CPE_{i\text{-}p}$ values for all MEAs were between 0.60 and 1. While no trend was seen in these values, $CPE_{i\text{-}p}$ values between 0.5 and 1 have been shown to represent a rough interface [35]. From analysis of the equivalent circuit model parameters, it is clear that inclusion of these heteropolyacids decreases the interfacial resistance.

3.4. Conclusions

Our experimental setup allowed us to independently control the water and DME flow rates. This led to an investigation of the optimal water:DME molar ratio, knowing that a 3:1 ratio is required by stoichiometry. While the optimal water:DME ratio will depend on all experimental conditions, it was found that, in general, a ratio higher than 3:1 was desirable. Other optimized experimental conditions were pressure, where 30 psig performed better than ambient pressures, and membrane thickness, where Nafion® 117 produced higher current densities than did Nafion® 112. Following the optimization study, 3 HPAs, phosphomolybdic acid, $H_3PMo_{12}O_{40}$, (HPMo), phosphotungstic acid, $H_3PW_{12}O_{40}$, (HPW), and silicotungstic acid, $H_4SiW_{12}O_{40}$, (HSiW) were incorporated into the anode catalyst layer in combination with Pt/C. HPW-Pt and HSiW-Pt produced higher current densities than the Pt control. Tafel slopes were extracted from anodic polarization data. At 30 psig, Tafel slopes of 67 mV dec^{-1}, 72 mV dec^{-1}, and 79 mV dec^{-1} were found for HPW-Pt, HSiW-Pt and the Pt control, respectively. At 0 psig, the Tafel slopes were 56 mV dec^{-1}, 58 mV dec^{-1}, and 65 mV dec^{-1} for HPW-Pt, HSiW-Pt and the Pt control. Electrochemical impedance spectroscopy was also performed, and the results are in agreement with the polarization trends. The addition of HPW more than doubled the power density of the fuel cell, compared to the Pt control. When the maximum power density obtained using the HPW-Pt MEA is normalized by the mass of Pt used, 78 mW mg^{-1} Pt is obtained. As is the case with the DMFC the addition of an opti-

mized HPA improves cell performance by 10%, this appears to be due to a combination of improved interfacial resistance in the MEA as well as improvements in electrocatalysis of the oxidation of the substrate.

Acknowledgement

This work was supported by the Xcel Energy Corporation by a grant from the Renewable Development Fund, Project No. CB07.

References

[1] M. Winter, R.J. Brodd, Chem. Rev. 104 (2004) 4245.
[2] M.M. Mench, H.M. Chance, C.Y. Wang, J. Electrochem. Soc. 151 (2004) A144.
[3] T.A. Semelsberger, R.L. Borup, H.L. Greene, J. Power Sources 156 (2006) 497.
[4] G. Kerangueven, C. Coutanceau, E. Sibert, J.M. Leger, C. Lamy, J. Power Sources 157 (2006) 318.
[5] Y. Tsutsumi, T. Satou, A. Yoshizawa, 12th International Symposium on Alcohol Fuels, Beijing, China, 1998.
[6] J.-Y. Im, B.-S. Kim, H.-G. Choi, S.M. Cho, J. Power Sources 179 (2008) 301.
[7] K.-D. Cai, G.-P. Yin, J. Zhang, Z.-B. Wang, C.-Y. Du, Y.-Z. Gao, Electrochem. Commun. 10 (2008) 238.
[8] J.H. Yoo, H.G. Choi, C.H. Chung, S.M. Cho, J. Power Sources 163 (2006) 103.
[9] R.H. Yu, H.G. Choi, S.M. Cho, Electrochem. Commun. 7 (2005) 1385.
[10] I. Mizutani, Y. Liu, S. Mitsushima, K.I. Ota, N. Kamiya, J. Power Sources 156 (2006) 183.
[11] S. Ueda, M. Eguchi, K. Uno, Y. Tsutsumi, N. Ogawa, Solid State Ionics 177 (2006) 2175.
[12] T. Haraguchi, Y. Tsutsumi, H. Takagi, N. Tamegai, S. Yamashita, Electr. Eng. Jpn. 150 (2005) 19.
[13] K.D. Cai, G.P. Yin, L.L. Lu, Y.Z. Gao, Electrochem. Solid State Lett. 11 (2008) B205.
[14] J.T. Muller, P.M. Urban, W.F. Holderich, K.M. Colbow, J. Zhang, D.P. Wilkinson, J. Electrochem. Soc. 147 (2000) 4058.
[15] L.M. Pan, Z.Y. Zhou, D.J. Chen, S.G. Sun, Acta Phys. Chim. Sin. 24 (2008) 1739.
[16] Y. Zhang, L.L. Lu, Y.J. Tong, M. Osawa, S. Ye, Electrochim. Acta 53 (2008) 6093.
[17] Y. Liu, S. Mitsushima, K. Ota, N. Kamiya, Electrochim. Acta 51 (2006) 6503.
[18] L.L. Lu, G.P. Yin, Y.J. Tong, Y. Zhang, Y.Z. Gao, M. Osawa, S. Ye, J. Electroanal. Chem. 619 (2008) 143.
[19] P. Piela, C. Eickes, E. Brosha, F. Garzon, P. Zelenay, J. Electrochem. Soc. 151 (2004) A2053.
[20] B.R. Limoges, R.J. Stanis, J.A. Turner, A.M. Herring, Electrochim. Acta 50 (2005) 1169.
[21] M.-C. Kuo, R.J.J.R.F. Stanis III, J.A. Turner, A.M. Herring, Electrochim. Acta 52 (2007) 2051.
[22] J.R. Ferrell III, M.-C. Kuo, J.A. Turner, A.M. Herring, Electrochim. Acta 53 (2008) 4927.
[23] R.J. Stanis, M.-C. Kuo, J.A. Turner, A.M. Herring, J. Electrochem. Soc. 155 (2008) B155.
[24] J.W. Chen, J. Zeng, C.P. Jiang, Y.H. Wang, B.J. Zhao, S.F. Zhu, R.L. Wang, Chin. J. Catal. 28 (2007) 725.
[25] A.M. Herring, Polym. Rev. 46 (2006) 245.
[26] J.J. Borrás-Almenar, E. Coronado, A. Müller, M.T. Pope (Eds.), Polyoxometalate Molecular Science, Kluwer Academic Publishers, Dordrecht, Boston, 2001.
[27] M. Sadakane, E. Steckhan, Chem. Rev. 98 (1998) 219.
[28] G.M. Brown, M.-R. Noe-Spirlet, W.R. Busing, H.A. Levy, Acta Cryst. B33 (1977) 1038.
[29] J.F. Keggin, Nature 131 (1933) 908.
[30] F.N. Buchi, D. Tran, S. Srinivasan, Electrochemical Society Proceedings, Chicago, IL, 1995.
[31] Kucernak, A.R.J., Barnett, C.J., Burstein, G.T., Williams, K.R., 1995. New Materials for Fuel Cell Systems I: Proceedings of the First International Symposium on New Materials for Fuel Cell Systems, Montreal.
[32] R.J. Stanis, M.C. Kuo, J.A. Turner, A.M. Herring, J. Electrochem. Soc. 155 (2008) B155.
[33] P. Heo, M. Nagao, M. Sano, T. Hibino, J. Electrochem. Soc. 155 (2008) B92.
[34] S.K. Roy, M.E. Orazem, J. Power Sources 184 (2008) 212.
[35] F. Berthier, J.-P. Diard, R. Michel, J. Electroanal Chem. 510 (2001) 1.